International Journal of Integrative sciences, Innovation and Technology
(A Peer Review E-3 Journal of S*cience* I*nnovation* T*echnology*)
Section A – Basic Sciences; Section B –Applied and Technological Sciences; Section C – Allied Sciences
Available online at www.ijiit.net

Research Article

SYNTHESIS AND CHARACTERISATION OF TUNGSTEN OXIDE ON NITROGEN DOPED GRAPHENE AND PERFORMANCE MEASUREMENT IN ALKALINE FUEL CELLS

A. KEDHARNATH, KV. HARI KRISHNAN, G. ARULKUMAR, R. PADMAVATHI, D. SANGEETHA*
Department of Mechanical Engineering, Anna University, Chennai-600 025, India
*Corresponding author E-mail: sangeetha@annauniv.edu

ABSTRACT
The development of non-noble support materials has the potential to reduce the cost and also increase the efficiency of fuel cells. Alkaline fuel cell (AFC) uses alkaline electrolyte membrane which has an advantage of using non noble metals as there is no corrosion problem due to acidic medium. Here we present tungsten oxide on nitrogen doped graphene for highly efficient anode reaction catalyst in alkaline fuel cells. In the current work, graphene oxide is synthesized using modified Hummer's process followed by hydro thermal treatment with urea resulting in nitrogen doped reduced graphene (NRG) and metal oxide are incorporated into NRG. The functional groups present on GO, NRG and metal oxide-incorporated NRG are confirmed using Laser Raman spectroscopy and FTIR. The structural studies are obtained by X-Ray Diffraction analysis. Morphology and compositional analyses are done using SEM with EDAX. Electro catalytic activities are studied for GO, NRG and WO_3-NRG using cyclic voltammetry (CV). The alkaline fuel cell performance showed the maximum power density for WO_3-NRG (93 mW cm^{-2} at 60 ^oC) and compared with commercially available Pt/C catalysts.

KEYWORDS: non noble metal, alkaline fuel cells, graphene, tungsten oxide

INTRODUCTION
Fuel cell system promises to be a great alternative for a range of applications from electronic appliances to high end automobiles [1]. Their potential to reduce the environmental impact and geopolitical consequences caused by the use of fossil fuels has made them a great alternative to the combustion engines. A fuel cell uses some sort of chemical fuel as its energy source; like a battery, the chemical energy is directly converted to electrical energy, without an often messy and relatively inefficient combustion step [2]. In addition to high efficiency and low emissions, fuel cells are attractive for their modular and distributed nature, and zero noise pollution. They will also play an essential role in any future hydrogen fuel economy. In the past few years, different types of fuel cells have been developed depending upon the type of the electrolyte used [3] such as direct methanol fuel cell (DMFC), phosphoric acid fuel cell (PAFC), proton exchange membrane fuel cell (PEMFC), solid oxide fuel cell (SOFC), and alkaline fuel cell (AFC). For low temperature fuel cell applications, PEMFC are found to be promising, due to its quick startup and high power density [4]. The most important advantage of alkaline fuel cells (AFCs) over their acidic counterparts is their greatly improved oxygen reduction kinetics as well as a better fuel oxidation kinetics [5]. These improvements can lead to higher efficiencies and enable the use of non-noble metal catalysts, greatly reducing the cost of the device. Indeed, hydrogen fueled AFCs can outperform all known low temperature fuel cells [6]. The primary components of a fuel cell are an ion conducting electrolyte, a cathode, and an anode. Together, these three are often referred to as the membrane-electrode assembly (MEA), or simply a single-cell fuel cell. In the simplest example: a fuel such as hydrogen is brought into the anode compartment and an oxidant, typically oxygen, into the cathode compartment. There is an overall chemical driving force for the oxygen and the hydrogen to react to produce water. Direct chemical combustion is prevented by the electrolyte that separates the fuel (H_2) from the oxidant (O_2) [7].

Fuel cells are still far from market launch, because of hindrance by two main issues: the prohibitive production cost and poor durability and reliability [8]. Catalysts exhibit great influence on both the cost and the durability of AFC. Most of the presently used catalysts are Pt-based and are usually supported on porous conductive materials with a high specific surface area. The support materials are necessary to

obtain a high dispersion and a narrow distribution of Pt and Pt-alloy nanoparticles, which is the prerequisite to obtain a high catalytic performance of catalyst [9]. The main objective in fuel cell systems is to develop high performance, low cost and durable materials – catalyst and membranes. Presently, fuel cells are too expensive and not much durable. There are many ways to improve the performance, simultaneously reducing the capital cost [10]. The alkaline membrane fuel cell technology slightly differs from the other fuel cell types, because of the two key components, one is anion exchange membrane and the second one is Pt-free catalyst.

Novel or non-noble catalyst materials are being increasingly researched as an alternative to the Pt-catalyst which is mainly used nowadays. Many conductive or semi-conductive oxides have been studied as catalyst support materials or as a secondary supports to modify and promote the catalyst support for fuel cells, including indium tin oxide (ITO), TiOx, WOx, IrO_2, SnO_2, and they have shown promising activity [11].
Tungsten oxide is an n-type semiconductor with a reported band gap of about 2.6 to 2.8 eV [12]. Because tungsten has many oxidation states from 2 to 6, it can exist in many forms, making it suitable for electro chromic, photo chromic, photo catalyst, and gas-sensor applications [13]. The intrinsic electric conductivity in tungsten oxide arises from its non-stoichiometric composition, giving rise to a donor level formed by oxygen-vacancy defects in the lattice [14]. Tungsten oxides can also be used as catalyst supports and they also exhibit enhanced catalytic activity for the electro oxidation of methanol [15]. These tungsten oxides also show high resistance to CO poisoning and contamination from H_2S [16]. All these oxides have a common advantage over carbon supports for extending electro catalyst life. In addition to the above-mentioned specific properties, when they are oxidized they still remain on the support in another form (e.g., metal hydrates). The intrinsic proton transfer property of some oxides provides a new pathway to design electro catalysts and support materials, which could not only increase the utilization of catalytic metals and enhance the catalytic activity, but also decrease fuel cell cost by lowering the usage of a Nafion ionomer.

Graphene, a novel material has attracted tremendous attention for its unusual electronic properties and possible application in various fields [17]. Its optical transmittance, large surface area and high electrical conductivity are valuable in promoting electron transfer in electrochemistry, solar cells, nanoelectronics, etc. [18].

Recently, graphene oxide (GO), prepared by Hummer's process [19] with strong oxidants and ultrasonic cleavage, has attracted much attention as a possible intermediate for manufacture of graphene in large volume. Some modifications have been performed to the oxidation process based on Hummers method [20]. This process is the modified Hummer's process. In addition, because of the large amount of oxygen-containing functional groups [21], the resulting product, obtained by the modified Hummer's process was less efficient than GO. Lerf and Klinowski proposed a structural model for GO prepared by Hummers, according to which GO contained two kinds of randomly distributed regions: aromatic regions with unoxidized benzene rings and regions with aliphatic six-membered rings. The relative size of the two regions depended on the degree of oxidation, with hydroxyl and epoxy groups located on the interior of GO and carboxyl (COOH) groups at the edges of layers.

In this article, we chose quaternized polystyrene ethylene butylenes polystyrene membrane [22], carbon supported platinum catalyst (Pt/C) and activated carbon supported tungsten oxide doped nitrogen reduced graphene (WO_3-NRG/C) as anode and cathode materials, respectively, to fabricate membrane electrode assembly (MEA).

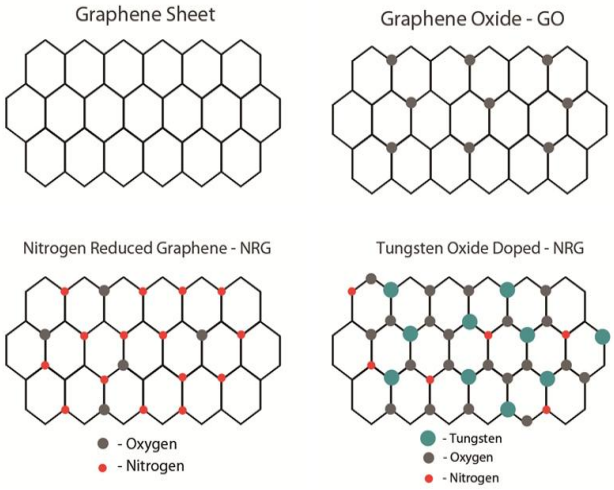

Scheme 1: Schematic representation of synthesized products (a) graphene sheet, (b) graphene oxide, (c) nitrogen reduced graphene and (d) tungsten oxide doped-NRG

EXPERIMENTAL

Synthesis of graphene oxide (GO)

Graphite powder was used as the starting material. Graphene oxide was first prepared by the oxidation of graphite powder using the modified Hummers' method [23]. Typically, graphite powder (2 g, purity degree Carbon: 99.5%, ~30 µm) and sodium nitrate (1g) were first stirred in concentrated sulphuric acid (46 mL) while being cooled in an ice water bath. Then potassium permanganate (6 g) was gradually added to form a new mixture. After 2 h in an ice water bath, the mixture was allowed to stand for 2 days at room temperature with gentle stirring. Thereafter, 100 mL of 5 wt% H_2SO_4 aqueous solution was added into the

above mixture over 1 h with stirring. Then, 20 ml of H_2O_2 (30 wt% aqueous solution) was also added to the above liquid and the mixture was stirred for 2 h. After that, the suspension was filtered and washed until the pH value of the filtrate was neutral. The as-received slurry is the so-called graphene oxide. Finally, the dried graphene oxide was obtained after heating in Teflon autoclave at 180 °C for 24 hrs. Nitrogen doped graphene was further obtained by hydrothermally reducing graphene oxide under high purity urea at 120 °C for 12 hrs [24].

Synthesis of nitrogen doped/reduced grapheme

The N-doped graphene nanosheets with high nitrogen content were synthesized through a one-pot hydrothermal process using urea as the chemical dopant in the presence of GO aqueous dispersion. Typically, 10 mL GO (40 mg) aqueous dispersion was diluted with 25 mL of deionized water, and then a given amount of urea was added into the GO dispersion under sonication for 3 h. After that, the solution was sealed in a 50 mL teflon-lined autoclave and maintained at 180 °C for 12 h. The solids (N-doped/reduced graphene) were filtered and washed with distilled water several times until neutrality is achieved [25].

Synthesis of tungsten oxide on nitrogen reduced grapheme

Tungsten oxide doped nitrogen reduced graphene (WO_3-NRG) was synthesized using an in-situ hydrothermal growth reaction. The typical process was, 25 mg of NRG obtained after hydrothermal reduction of GO obtained using modified Hummer's process was taken, and dissolved in 10 ml distilled water. This mixture was sonicated for about 15-20 min for homogenous mixing. Then 0.2g NaCl and 1g of $Na_2WO_3.2H_2O$ (Sodium Tungstate dehydrate, purified), were added into the mixture and then ultrasonicated or stirred for continuously 6 hrs. The pH of the mixture was increased to 2 by adding conc. HCl. Then hydrothermal reaction was done inside a Teflon Autoclave at 180 °C for 24 hrs. The resulting solution was centrifuged at 3500 rpm for about 30 min till the solution got neutralized. It was then dried in an oven at 80 °C for 24hrs [26].

Materials characterization

Morphological studies

The morphology of the obtained catalyst is obtained using scanning electron microscopy. The images are taken from Carl Zeiss MA15/EVO 18 which has Tungsten hairpin filament with Oxford Instruments Nano Analysis INCA Energy 250 Microanalysis System (EDS) with 130eV INCAx-act Peltier cooled Analytical SDD Detector with PentaFET® Precision having capability of Quantitative, Qualitative, mapping, Point & ID etc. including cobalt standard on pin stub. The sample was sputtered with gold and palladium. The morphology of the sample was viewed at a magnification of 50,000 with signals from secondary electrons.

Compositional analysis

The composition of the synthesized catalyst were found using Energy Dispersive X-ray Analysis. The images were taken from Carl Zeiss MA15 / EVO 18 which has Tungsten hairpin filament with Oxford Instruments Nano Analysis INCA Energy 250 Microanalysis System (EDS) with 130eV INCAx-act Peltier cooled Analytical SDD Detector with PentaFET® Precision having capability of Quantitative, Qualitative, mapping, Point & ID etc. including cobalt standard on pin stub. The characteristic X-rays with various KeV from the samples were analysed to find the composition of the film. The elemental compositions were analyzed using characteristic X-rays coming from the respective material due to electron material interaction. Usually Kα, Lα, Kβ, Lβ characteristic X-rays were collected which have their own energy (KeV) and were counted using Miller counter. There were also peaks of other materials which were not in the specimen. This way be due to the overlap of energies of Lα and Kβ of one material by another material.

Phase Analysis

The phase analysis and crystallographic nature of the synthesized material was obtained using X-Ray Diffraction (XRD) analysis. High Resolution X-Ray diffraction (HR-XRD) was done in PAN analytical X-Pert Pro MRD Resolution 0.0001°/0.36 arc sec Ge-(220) monochromator Triple axis (Xe) detector Pixel detector. Empyrean XRD tube Cu LFF HR DK327806 was used to produce Kα1 (Å): 1.540598. The scan mode is theta/2theta with minimum step size 2theta: 0.0001 and minimum step size Omega: 0.0001 with a scan range of: 20-60^o.

Raman spectroscopy

The Raman spectra were recorded based on Raman R3000 System and by using a 509 working-length objective (8 mm). The exciting wavelength was 532 nm with radiation from a He–Ar laser with a power of 0–90 mW at the surface of the sample and a spot of ca. 3 lm on the sample surface. The prepared samples of GO, NRG and WO_3-NRG were placed in a specially designed quartz in situ Raman sample cell.

FTIR

The functional groups present in the synthesized samples of GO, NRG and WO_3-NRG were analysed using Bruker analyzer. For background elimination and baseline correction, initially KBr sample was pelletized and analysed for functional groups. This observation was kept as reference for the analysis of the synthesized samples. Each powder was mixed with KBr in a 1: 20 ratio and pelletized. This was kept in the sample holder and IR rays were passed and the results are obtained.

Cyclic voltammetric study

Electrochemical measurements were carried out an electrochemical workstation with a standard three-electrode system (Ag/AgCl as reference electrode, Pt as counter electrode and Glassy Carbon as working electrode (GC, 3 mm diameter)). The solutions were purged with nitrogen for at least 15 min to remove oxygen. The metal oxide WO_3-NRG to be used as electrode were prepared by mixing as-prepared samples dispersed in distilled water (1.0 mg mL^{-1}). Then the solution (20 mL) was applied onto pre-polished glassy carbon electrodes and allowed to dry in air. 20 mL of 0.5 wt% Nafion was then cast on the above glassy carbon electrodes and dried in air. Cyclic voltmeter shows the variation of current with potential [27].

Fabrication of MEA and AFC performance study

Two sets of MEAs using Pt/C and WO_3-NRG with QPSEBS membrane were prepared as reported in our previous literature [28]. The fuel cell tests were carried out using in-house fuel cell test station. Membrane electrode assemblies (MEAs), 25 cm^2 were produced by hot pressing. The MEA was secured between two graphite plates which had machined triple serpentine flow channels (1 mm channel width, 1 mm channel height, and 1.5 mm rib width) and gold coated aluminium current collector plates. The fixture was sealed at a constant torque of 5.5 Nm, using bolts and a torque wrench. Fuel cell measurements were carried out at 60 °C with H_2 and O_2 gases.

RESULT AND DISCUSSION

Morphology studies

The SEM images of (a) GO, (b) NRG and (c) WO_3-NRG are shown in Fig. 1. The layers of GO were found to be so closer to each other that they were very difficult to distinguish. Doping nitrogen increased the distanced between the layers. The distance between the layers was approximately 200 nm. WO_3 can take different morphology such as nano rods/wire, hexagonal platelets or square nano sheets depending upon the use of solvent like ethanol, water & ethanol and water respectively. The current researched clearly that the morphology is nano rods/wires like structure forming clusters and tangled [29]. Doping of tungsten oxide to NRG gave a different morphology than GO and NRG. There was formation of nano rods of WO_3-NRG composite with high aspect ratio on the NRG structure. The nano rods were approximately 50 nm in diameter. There was no homogeneity in distribution of nano rods. There was some clustering of nano rods in which they entangled with each other. This confirmed the doping of WO_3 on NRG.

Fig 1: SEM morphology of (a) GO, (b) Nitrogen reduced graphene and (c) Tungsten doped NRG

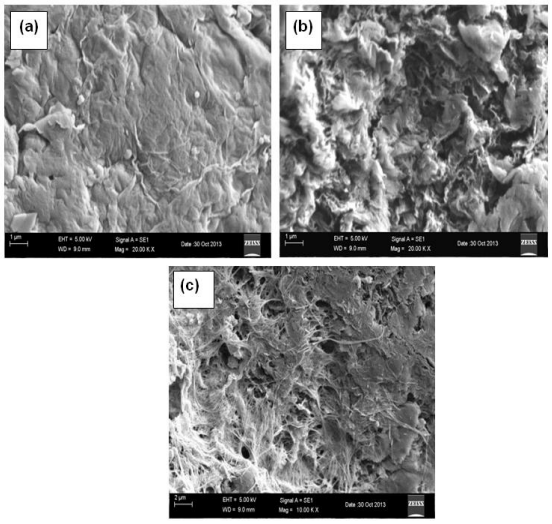

Compositional analysis

The EDAX confirmed the presence of carbon and oxygen in GO, nitrogen, carbon and oxygen in NRG and tungsten, oxygen, carbon and nitrogen in WO_3-NRG as shown in Fig. 2.

Fig 2: Compositional analysis of (a) GO, (b) Nitrogen reduced graphene and (c) Tungsten doped NRG using EDAX

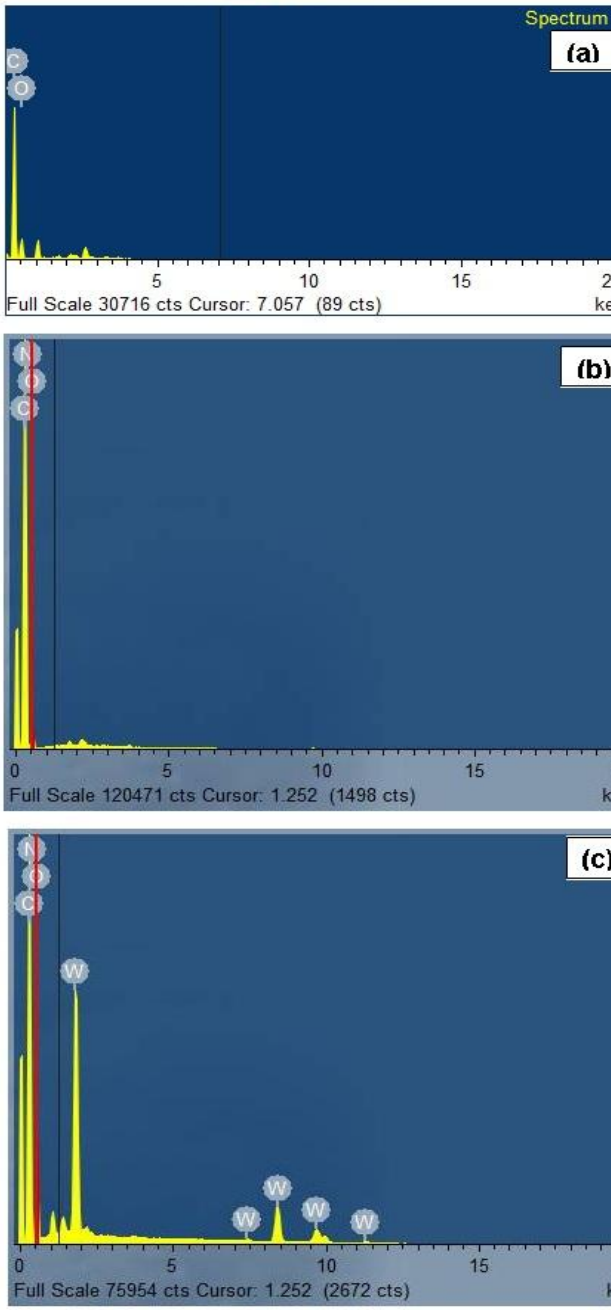

Phase analysis

The XRD shown in Fig.3 proved the formation of GO and NRG by showing a peak at 10.4° (2 Theta) and 28° respectively. After doping of nitrogen there was a shift of peak from 10.4° to 28°. Doping of tungsten produced many peaks of tungsten oxide (WOx). In the XRD plot of tungsten oxide-NRG, the peaks below 30°, showed the peaks of GO and NRG. Their crystal structure also varies depending on their morphology. Use of ethanol or water gives nano rods/wire or square nano sheets with monocline crystal structure while using both ethanol and water gives hexagonal platelet like structure with hexagonal structure. It is also clear that the formed nano rods/wires of WO_3 are monoclinic structures grown majorly on {202} planes [29].

Fig 3: Phase analysis of (a) GO, (b) Nitrogen reduced graphene and (c) Tungsten doped NRG using X-ray Diffraction

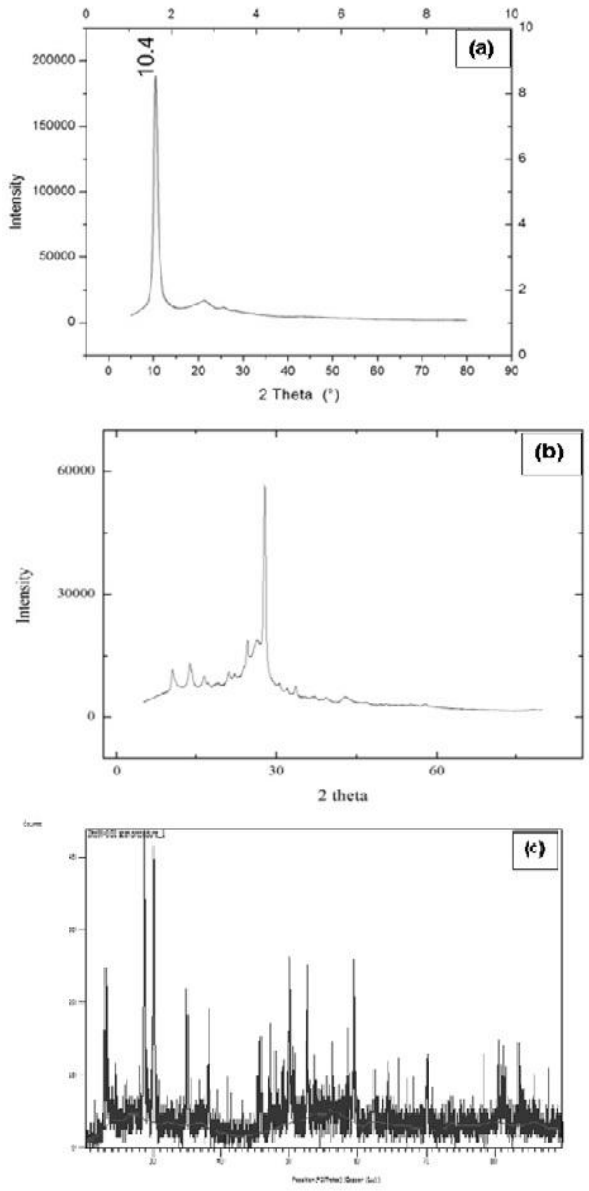

Raman spectrum analysis

Raman spectroscopy of (a) GO, (b) NRG and (c) Tungsten doped NRG is shown in Fig. 4. The synthesised GO analysed using laser Raman Spectrometer shows two peaks at 1599 cm^{-1} and 1352 cm^{-1} which are G band and D band, respectively. The G peak position shifted from 1599 cm^{-1} for GO to 1589 cm^{-1} for NRG. This is an ideal graphitic lattice vibration mode with E_{2g} symmetry, and thereby characterizes the highly ordered graphite carbon materials. Interestingly, the G peak of NGR further shifted to 1580 cm^{-1}. The downshift of the G peak in NGR was consistent with the report, signifying the successful N doping. The D band (or ‘‘Defect” band) at 1352 cm^{-1} was the characteristic of disordered graphite

and corresponds to a graphitic lattice vibration mode with A_{1g} symmetry. The peak shift in WO_3-NRG is similarly due to the interaction of WO_3 with graphene layers and also there is disorder of sp^2 contribution by the presence of WO_3. The I_D/I_G intensity ratio is an index of the disorder degree and the average size of the sp^2 domains. The I_D/I_G intensity ratio decreased slightly from 1.2 (for graphite) to 0.97 and 0.93 for GO and NRG samples, respectively, thereby providing evidence that the graphene structure was essentially restored upon the chemical reduction. After doping tungsten oxide, the D and G bands have come closer and the peaks superimpose [26].

Fig4: Raman shift analysis of (a) GO, (b) Nitrogen reduced graphene and (c) Tungsten doped NRG

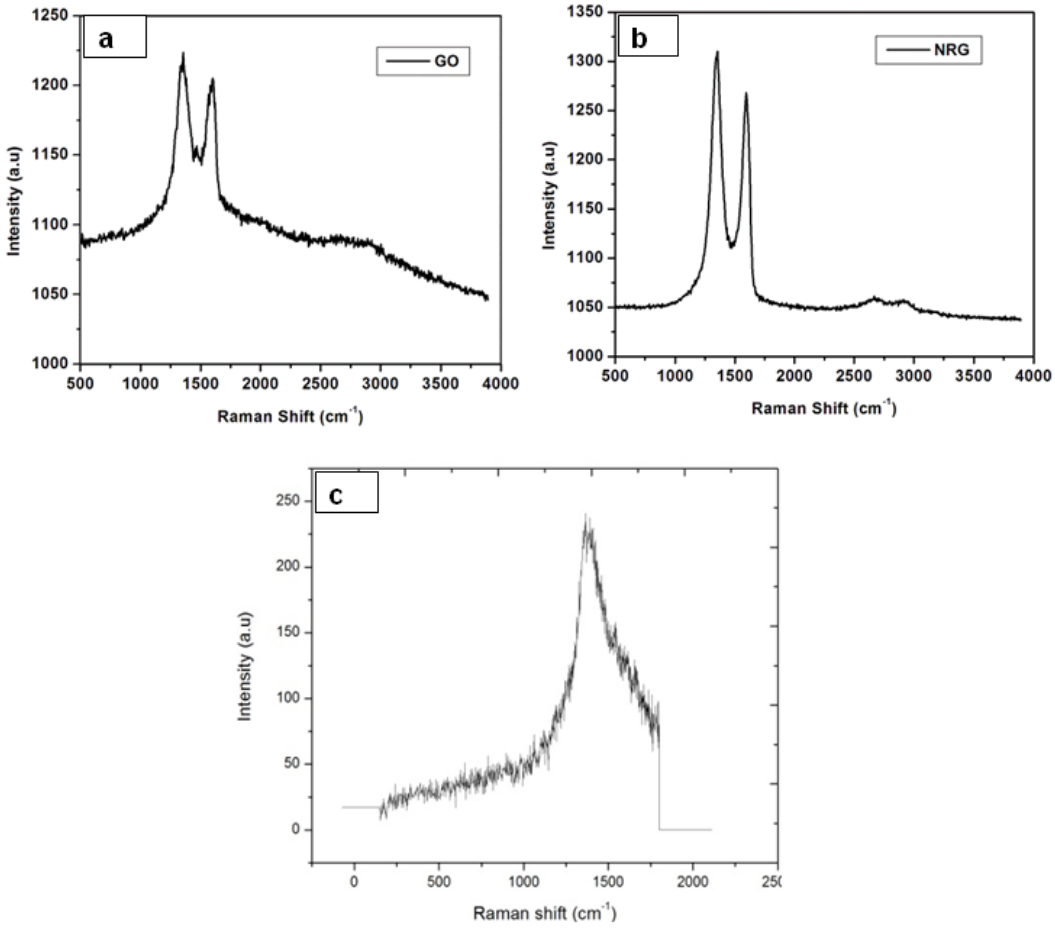

Functional group analysis

The FTIR images of (a) GO, (b) NRG and (c) Tungsten oxide doped NRG are shown in Fig.5. The difference in the transmittance was due to the sp^2 hybridization of GO and this varied when nitrogen was doped into it. The number of active sites in NRG was useful in doping tungsten oxide. There was more relation between GO and WO_3-NRG while NRG showed a wide difference in transmittance. The Infrared spectra results of the compounds synthesized are shown in GO: it is clearly observed that the absorption peak at 3300-3700 cm^{-1} can be ascribed to the stretching of the –OH bonds. The appearance of the characteristic peak at 1116 cm^{-1} shows C-O stretching, and the peak at 1389 cm^{-1} was due to the vibration of C-N bonds. The other small peaks in the spectra correspond to the presence of other functional groups like carboxyl, carbonyl present in GO. NRG: The difference between the GO and NRG is the presence of the dopant, Nitrogen in the latter. In the spectra obtained, the C-O peak (1116 cm^{-1}) which was predominant in GO has been masked by the C-N group at 1731 cm^{-1} due to nitrogen doping of the GO leading to formation of NRG. The spectra also showed small amount of –OH group present in the compound (peaks at 3300 – 3700 cm^{-1}). WO_3-NRG: Due to the increased content of the metal oxide of the NRG (by doping), the peaks for the absorption bands became stronger and shifted to lower wavenumbers. The peak obtained for NRG at 1731 cm^{-1} shifted to peak at 795 cm^{-1} which confirmed the presence of metal oxide in the compound. The other significant peaks of C-O, C-N, and the –OH which were seen earlier, has been

completely masked by the presence of metal oxide. This showed that the reaction was proper and the metal oxide has been loaded into NRG [26, 29].

Fig 5: Fourier Transform Infrared Spectroscopy of (a) GO, (b) NRG, and (c) Tungsten doped NRG

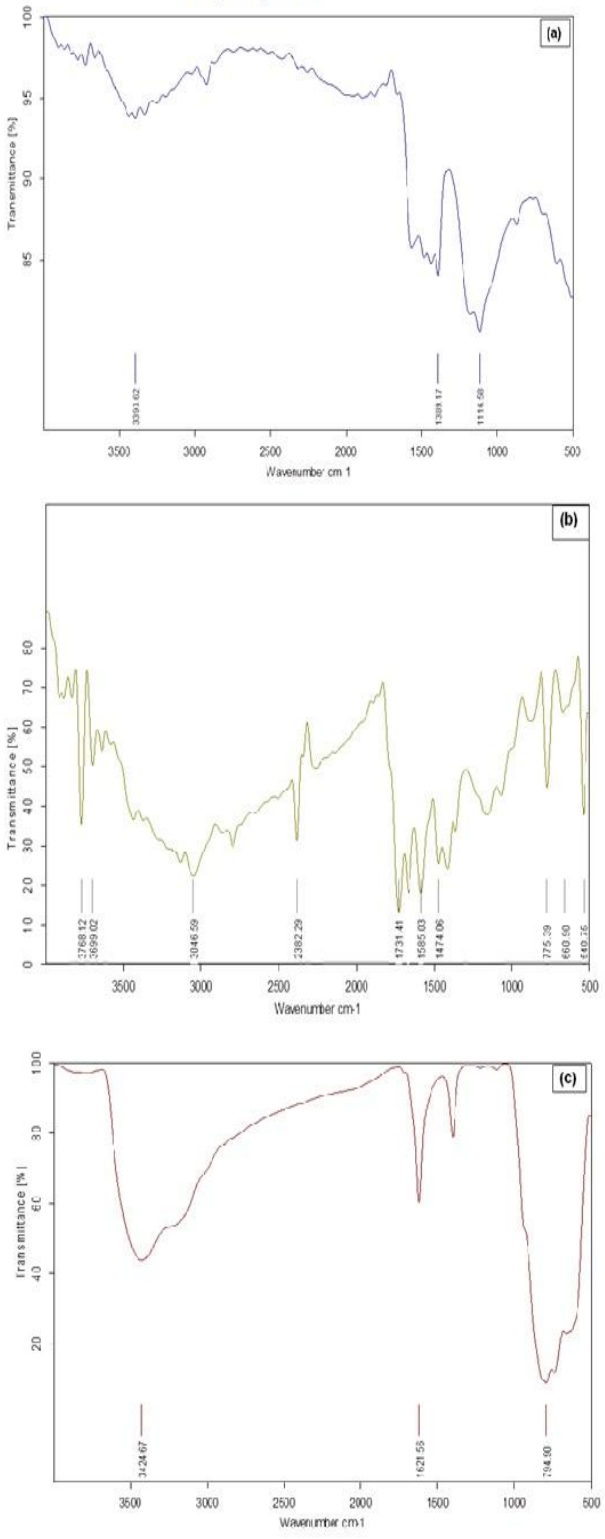

Cyclic voltammetric analysis

The cyclic voltammetry analysis of (a) GO, (b) NRG and (c) Tungsten doped NRG is shown in Fig.6. In the CV studies, for a compound with no activity, there is no loop in the graph. But here the samples of GO, NRG and WO_3-NRG all showed loops in the graph. The variation for GO was from -10 to 8 mA, while for NRG and WO_3-NRG were from -4.5 to .5 mA and -0.5 to 0.25 mA, respectively. The synthesized WO_3-NRG clearly showed the electro-catalytic activity of the electrode [30-31].

Fig 6: CV studies of (a) GO, (b) Nitrogen doped reduced graphene, and (c) Tungsten doped NRG

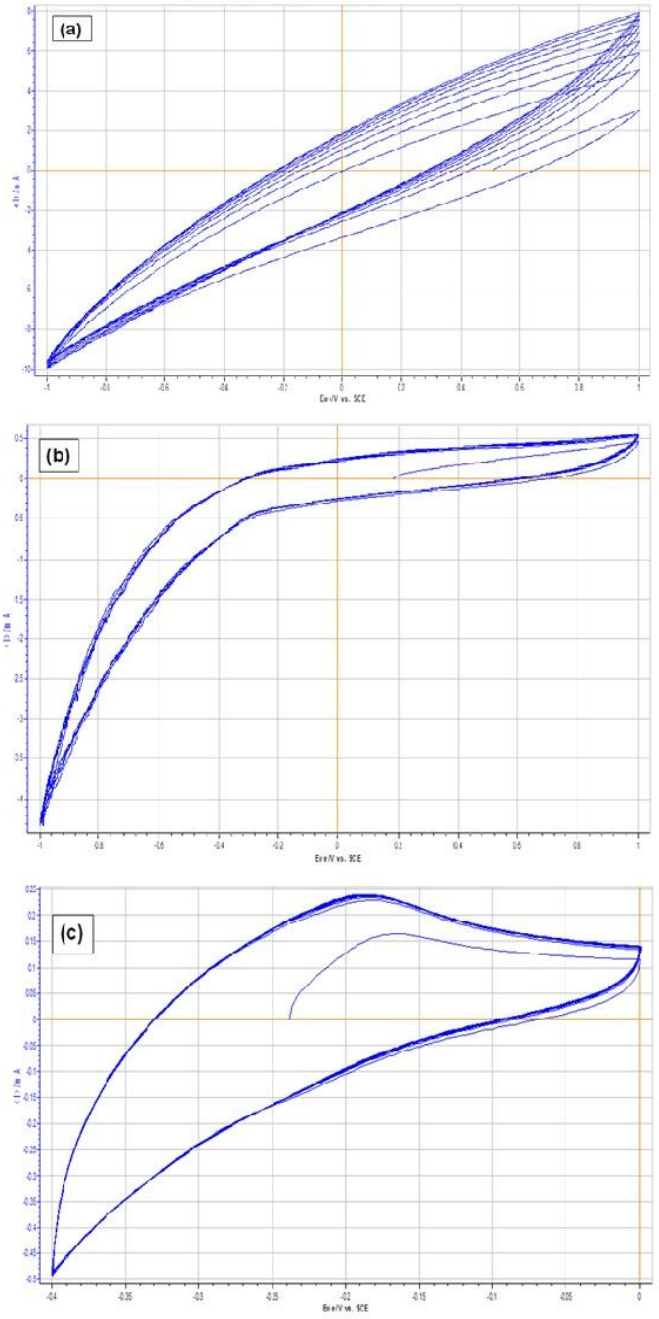

Performance measurement

The polarization and power density curves of synthesized samples, obtained from the alkaline membrane fuel cell using Pt as the anode and WO_3-

NRG as catalyst are presented in Fig.7. The measurements were made by feeding hydrogen and oxygen as a fuel and oxidant, respectively, at 60 °C. At low currents the region of activation polarization loss can be distinguished on the cell voltage curve, related to slow kinetics of the oxygen reduction reaction. At intermediate currents a region of ohmic polarization loss is observed and finally, at higher currents the concentration polarization loss leads to a gradual decrease of the cell voltage. The alkaline membrane fuel cell with WO_3-NRG showed a maximum cell voltage of 0.720V and power density of 93 mW cm^{-2} at 60 °C. Pt/C produced a maximum voltage of 0.750 V and power density of 112 mW cm^{-2} at 60°C.

Fig 7: Single cell alkaline fuel cell performance of (a) Pt/C and (b) WO_3/NRG

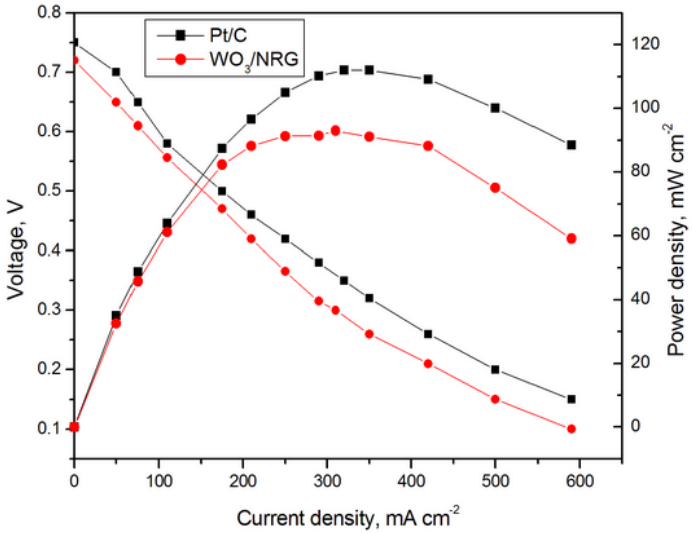

CONCLUSION

This work deals with the development of electrode for alkaline fuel cells using only non-noble metal and to increase the performance of the fuel cells. The synthesised graphene oxide, nitrogen reduced graphene and tungsten doped graphene was confirmed by FTIR and their crystalline nature were confirmed by XRD. The morphology proved the increased interlayer distance and also the elemental composition were confirmed the presence of Tungsten (W). The Raman spectroscopy WO_3-NRG slightly shifted due to the interaction of WO_3 with graphene layers and also there is disorder of sp^2 contribution by the presence of WO_3. In the present work, nitrogen reduced GO doped with WO_3-NRG was produced by simple process and the product can be used as an efficient cost effective electrode to increase the performance of Alkaline Fuel cells.

ACKNOWLEDGEMENTS

The authors would like to thank CSIR, India (vide letter no. 01(2452)/11/EMR-II dated 16.05.2011) for their financial assistance to carry out the research work is greatly acknowledged.

REFERENCES

1. *H.A.Gasteiger, S.S.Kocha, B.Sompalli, F.T.Wagner; Applied Catalysis B: Environmental, 56, 9-35 (2005)*
2. *Sammes N (2006) Fuel cell technology: reaching towards com- mercialization. Springer, London, Blomen LJMJ, Mugerwa MN (1993) Fuel cell systems. Plenum Press, New York, Mench MM (2008) Fuel cell engines. John Wiley and Sons Ltd., London, Hermanna A, Chaudhuria T, Spagnol P (2005) Int J Hydrogen Energy).*
3. *Steele BCH, Heinzel A (2001) Nature 414:345*
4. *L.Carrette, K.A.Friedrich, U.Stimming; Chemical Physics and Physical Chemistry, 1, 5 – 39 (2001)*
5. *G.F.Mc Lean, T.Niet, S.Prince-Richard, N.Djilali; International Journal of Hydrogen Energy, 27, 507– 526 (2002).*
6. *J.R.Varcoe, R.C.T.Slade; Fuel Cells, 5, 187–200 (2005)*
7. *Sossina M. Haile, Fuel cell materials and components, Acta Materialia 51 (2003) 5981–6000)*
8. *R. Borup, J. Meyers, B. Pivovar, Y. S. Kim, R. Mukundan, N. Garland, D. Myers, M. Wilson, F. Garzon, D. Wood, P. Zelenay, K. More, K. Stroh, T. Zawodzinski, J. Boncella, J. E. McGrath, M. Inaba, K. Miyatake, M. Hori, K. Ota, Z. Ogumi, S. Miyata, A. Nishikata, Z. Siroma, Y. Uchimoto, K. Yasuda, K. I. Kimijima and N. Iwashita, Chem. Rev., 2007, 107, 3904–3951.*
9. *Y. Y. Shao, G. P. Yin and Y. Z. Gao, J. Power Sources, 2007, 171, 558–566*
10. *Harper GDJ (2008) Fuel cell projects for the evil genius. McGraw-Hill/TAB Electronics, London, Srinivasan S (2006) Fuel cells: from fundamentals to applications. Springer, New York*

11. *K. W. Park, K. S. Ahn, Y. C. Nah, J. H. Choi and Y. E. Sung, J. Phys. Chem. B, 2003, 107, 4352–4355.*
12. *S. H. Lee, R. Deshpande, P. A. Parilla, K. M. Jones, B. To, A. H. Mahan and A. C. Dillon, Adv. Mater., 2006, 18, 763–766.*
13. *H. Chhina, S. Campbell and O. Kesler, J. Electrochem. Soc., 2007, 154, B533–B539*
14. *S. Supothina, P. Seeharaj, S. Yoriya and M. Sriyudthsak, Ceram. Int., 2007, 33, 931–936.*
15. *P. J. Barczuk, H. Tsuchiya, J. M. Macak, P. Schmuki, D. Szymanska, O. Makowski, K. Miecznikowski and P. J. Kulesza, Electrochem. Solid State Lett., 2006, 9, E13–E16.*
16. *J. B. Christian, S. P. E. Smith, M. S. Whittingham and H. D. Abruna, Electrochem. Commun., 2007, 9, 2128–2132.*
17. *Liang M, Zhi L (2009) J Mater Chem 19:5871*
18. *S. Guo and S. Dong, Chem. Soc. Rev., 2011, 40, 2644.*
19. *Hummers WS, Offeman RE (1958) J Am Chem Soc 80:1339*
20. *Zhang L, Li X, Huang Y, Ma YF, Wan XJ, Chen YS (2010) Carbon 48:2367.*
21. *Kovtyukhova NI, Ollivier PJ, Martin BR, Mallouk TE, Chizhik SA, Buzaneva EV, Gorchinskiy AD (1999) Chem Mater 11:771.*
22. *Rajangam Vinodh, Rajangam Padmavathi, Dharmalingam Sangeetha, Desalination 267 (2011) 267–276.*
23. *Hummers WS, Offeman RE (1958) J Am Chem Soc 80:1339. Zhang L, Li X, Huang Y, Ma YF, Wan XJ, Chen YS (2010) Carbon 48:2367.*
24. *H.C. Schniepp, J.-L. Li, M.J. McAllister, H. Sai, M. Herrera-Alonso, D.H. Adamson, R.K. Prud'homme, R. Car, D.A. saville, I.A. Aksay, J. Phy. Chem. B 110 (2006) 8535–8539.*
25. *Li Sun, Lei Wang, Chungui Tian, Taixing Tan, Ying Xie, Keying Shi, Meitong Li and Honggang Fu, RSC Advances, 2012, 2, 4498–4506*
26. *Xiaoqiang An, Jimmy C. Yu, Yu Wang, Yongming Hu, Xuelian Yu and Guangjin Zhang, J. Mater. Chem., 2012, 22, 8525.*
27. *Rajangam Padmavathi, Rajendhiran Karthikumar, Dharmalingam Sangeetha, Electrochimica Acta 71 (2012) 283-293.*
28. *Rajangam Padmavathi, Rajendhiran Karthikumar, Dharmalingam Sangeetha, Electrochimica Acta 71 (2012) 283.*
29. *Guo, Jingjing Li, Yao Zhu, Shenmin Chen, Zhixin Liu, Qinglei Zhang, Di Moon, Won-Jin Song, Deok-Min., RSC Advances, 2012, 2, 1356–1363.*
30. *Antolini, Ermete, Gonzalez, Ernesto R., Tungsten-based materials for fuel cell applications, Applied Catalysis B: Environmental, 96 (2010) 245–266.*
31. *Jayaraman, Shrisudersan, Jaramillo, Thomas F, Baeck, Sung-hyeon, Mcfarland, Eric W, J. Phys. Chem. B 2005, 109, 22958-22966.*